Neural correlates of conscious tactile perception: An analysis of BOLD activation patterns and graph metrics

Martin Grund[1], Norman Forschack[1,2], Till Nierhaus[1,3], and Arno Villringer[1,4]

[1]Department of Neurology, Max Planck Institute for Human Cognitive and Brain Sciences, 04103 Leipzig, Germany

[2]Experimental Psychology and Methods, Faculty of Life Sciences, University of Leipzig, 04109 Leipzig, Germany

[3]Neurocomputation and Neuroimaging Unit, Department of Education and Psychology, Freie Universität Berlin, 14195 Berlin, Germany

[4]MindBrainBody Institute, Berlin School of Mind and Brain, Charité – Universitätsmedizin Berlin and Humboldt-Universität zu Berlin, 10099 Berlin, Germany

Corresponding author: Martin Grund, Max Planck Institute for Human Cognitive and Brain Sciences, Stephanstr. 1A, 04103 Leipzig, Germany (mgrund@cbs.mpg.de)

Number of pages: 51

Number of *figures:* 12; *tables:* 4

Number of words for *Abstract:* 249; *Introduction:* 991; *Discussion:* 1963

Conflict of interest: The authors declare no competing financial interest.

Acknowledgements: The research was funded by the Max Planck Society. We thank Ramona Menger, Anke Kummer, Mandy Jochemko, and Nicole Pampus for their data acquisition support; Bettina Johst, Hendrik Grunert, and Jöran Lepsien for their technical advice; Heike Schmidt-Duderstedt and Kerstin Flake for preparing the figures for publication; and Joshua Grant for proofreading and commenting.

Abstract

Theories of human consciousness substantially vary in the proposed spatial extent of brain activity associated with conscious perception as well as in the assumed functional alterations within the involved brain regions. Here, we investigate which local and global changes in brain activity accompany conscious somatosensory perception following electrical finger nerve stimulation, and whether there are whole-brain functional network alterations by means of graph metrics. Thirty-eight healthy participants performed a somatosensory detection task and reported their decision confidence during fMRI. For conscious tactile perception in contrast to undetected near-threshold trials (misses), we observed increased BOLD activity in the precuneus, the intraparietal sulcus, the insula, the nucleus accumbens, the inferior frontal gyrus and the contralateral secondary somatosensory cortex. For misses compared to correct rejections, bilateral secondary somatosensory cortices, supplementary motor cortex and insula showed greater activations. The analysis of whole-brain functional network topology for hits, misses and correct rejections, did not result in any significant differences in modularity, participation, clustering or path length, which was supported by Bayes factor statistics. In conclusion, for conscious somatosensory perception, our results are consistent with an involvement of (probably) domain-general brain areas (precuneus, insula, inferior frontal gyrus) in addition to somatosensory regions; our data do not support the notion of specific changes in graph metrics associated with conscious experience. For the employed somatosensory submodality of fine electrical current stimulation, this speaks for a global broadcasting of sensory content across the brain without substantial reconfiguration of the whole-brain functional network resulting in an integrative conscious experience.

Keywords: somatosensory processing, perceptual awareness, consciousness, functional connectivity, graph theory, fMRI

Introduction

In the debate on the neural correlates of consciousness, several crucial issues are still not resolved. First, regarding the involved brain regions, some studies assume only areas related to the particular perceptual modality to be necessary (Auksztulewicz et al., 2012; Schröder et al., 2019), others emphasize the role of a parietal hot zone (Boly et al., 2017; Koch et al., 2016) whereas some theories - most notably the global workspace theory (Baars, 1988; Dehaene et al., 2006; Mashour et al., 2020) - assume conscious experience to depend on the involvement of widespread particularly fronto-parietal brain regions (Naghavi and Nyberg, 2005; Rees et al., 2002). Second, regarding the neurophysiological processes occurring *within* the involved brain regions, recent studies are suggesting specific alterations in their connectivity which can be identified by effects of transcranial stimulation (Casali et al., 2013) or using graph-theoretical metrics on fMRI data (Godwin et al., 2015; Sadaghiani et al., 2015).

For the somatosensory domain, previous fMRI activation studies have suggested the ipsilateral and contralateral secondary somatosensory cortices as the most promising candidates for conscious tactile perception (Moore et al., 2013; Schröder et al., 2019). Furthermore, recurrent interaction of S2 with S1 may play an important role for tactile detection (Auksztulewicz et al., 2012). Research focusing on tactile illusions has shown that S1 is activated somatotopically in correspondence with the illusory percept and body ownership (Blankenburg et al., 2006; Martuzzi et al., 2015). In this context, the temporal parietal junction (TPJ) plays a major role for bodily self-consciousness (De Ridder et al., 2007; Ionta et al., 2014). The insula has been consistently reported to be associated with conscious tactile perception (Moore et al., 2013) and described as a central hub for interoception (Ronchi et al., 2015) and self-identification (Park and Blanke, 2019). Interestingly, in another recent study, the insula together with anterior cingulate cortex coded for uncertainty across stimulation intensities (Schröder et al., 2019). In the same

study, frontal and parietal activations in tactile detection paradigms have been interpreted as serving the task (e.g., reporting a percept) but not the conscious sensory experience (Schröder et al., 2019). Yet, the above-mentioned ideas of a "global workspace" involving mainly fronto-parietal activity (Dehaene et al., 2006), or of a posterior cortical hot zone integrating sensory cortices (Koch et al., 2016) are conceived to be domain-general thus also applying to the tactile consciousness.

While most of the above-mentioned studies relied on the analysis of BOLD activation patterns, the question, whether functional connectivity changes or not, can be assessed using graph metrics (Bassett and Sporns, 2017). For this purpose, cortical and subcortical regions of interest (ROIs) are defined as nodes and their temporal relationships as edges (i.e., their connection; Bullmore and Bassett, 2011). The resulting network topologies are assessed with graph-theoretical measures such as modularity and clustering coefficient and compared between aware and unaware target trials (Godwin et al., 2015; Sadaghiani et al., 2015; Weisz et al., 2014). *Modularity* captures the global organization of nodes in subnetworks, whereas the *clustering coefficient* indicates whether a node's neighbors are also connected, thus forming local clusters. Measures of integration (e.g., *characteristic path length*) describe the general connectivity between all nodes, whereas measures of centrality (e.g., *participation coefficient*) reveal important nodes in the network. In this framework, visual awareness has recently been suggested to be accompanied by a decreased modularity and increased participation coefficient of the post-stimulus network topology in fMRI (Godwin et al., 2015). Importantly, these topologies had explanatory power beyond local BOLD amplitudes and baseline functional connectivity (Godwin et al., 2015). Globally, this indicates a lower segregation of nodes into distinct networks and locally a higher centrality of all nodes. A more integrated state accompanying stimulus awareness (Godwin et al., 2015) is supposed to facilitate broadcasting of sensory information to other brain areas (Dehaene et al., 2006; Dehaene

and Changeux, 2011). These widespread changes in functional connectivity have been interpreted as evidence supporting global models of awareness, e.g., the global workspace theory (Dehaene et al., 2006; Dehaene and Changeux, 2011). Whether these changes in graph metrics generalize to other sensory modalities is not yet answered.

In the present study, building on our previous experience in studies on neural processes underlying conscious and unconscious somatosensory processing (Blankenburg et al., 2003; Forschack et al., 2020; 2017; Nierhaus et al., 2015; Schubert et al., 2006), we used a “classical” fMRI detection paradigm in which aware and unaware trials of physically identical near-threshold stimuli are contrasted (Aru et al., 2012; Baars, 1988). Notably, our fMRI paradigm included a nine-second pause between stimulation and report, which made the assessment of functional network topologies with graph metrics possible. Therefore, our study design allowed to assess BOLD activity patterns and graph metrics independently, as well as to relate the two measures directly.

Two other features of our paradigm are important: (i) a confidence rating was included for each trial allowing for an analysis of confident decisions only and (ii) the paradigm included 25% catch trials. By comparing the contrast of undetected stimuli to correctly rejected catch trials, neural processes associated with non-conscious stimulus processing of near-threshold stimuli can be assessed. In a previous study on subthreshold stimuli, we had shown that they were associated with a deactivation of somatosensory brain regions (Blankenburg et al., 2003); however, it is not clear whether this is also true for stronger stimuli near the detection threshold.

Thus, our study aimed to address the following main questions:

- Do BOLD activation patterns following somatosensory near-threshold stimuli match the predictions of major consciousness theories, i.e., does the contrast detected/undetected lead to increased activity only in somatosensory areas (Schröder et al., 2019), in a fronto-parietal network (global workspace theory), or in a more restricted temporo-parietal-occipital hot zone (Koch et al., 2016)?
- Do graph metrics change with the conscious experience of somatosensory stimuli as shown for the visual system by Godwin et al. (2015), and do the affected areas match activated brain areas?
- Which neural changes are associated with non-perceived, but near-threshold somatosensory stimuli?

Materials & Methods

Participants

Thirty-eight healthy humans (19 women; mean age = 27.3, age range: 23-36) participated in the study. They had normal or corrected-to-normal vision and were right-handed (mean laterality index = 85, range: 60-100; Oldfield, 1971).

Ethics statement

All participants provided informed consent (including no contra-indication for MRI), and all experimental procedures were approved by the ethics commission at the medical faculty of the University of Leipzig.

Experimental design and statistical analysis

The experimental design of the tactile detection task had the intention to generate different sensory experiences for physically identical stimulus presentations. Brain activity accompanying these sensory experiences was sampled with BOLD fMRI (see fMRI data acquisition for details). The tactile stimulation was applied as a single electrical pulse to the left index finger. The stimulation intensity was set to the individual sensory threshold, before each of the four acquisition blocks, such that participants reported a stimulus detection (“hit”) in about 50% of the trials. One hundred near-threshold trials were intermingled with 20 clearly perceivable, supra-threshold trials and 40 catch trials without stimulation as control conditions. Participants had to report their perception (yes/no) and decision confidence (see “behavioral paradigm” for details). This led to three within-participant factors of interest: (a) rejected catch trials without stimulation (correct rejections), (b) non-perceived near-threshold trials (misses), and (c) perceived near-threshold trials (hits). We did not include false alarms (reported “yes” in catch trials without

158 stimulation) due to the low false alarm rate (mean FAR = 3.3%, *SD* = 6.0%). 17 of 31
159 participants reported zero false alarms.

160 We compared the graph metrics between hits, misses and correct rejections across
161 participants with the Wilcoxon's signed-rank test (see Graph-theoretical analysis for
162 details). For each graph metric, the *p*-values of the 24 paired Wilcoxon's signed-rank tests
163 were corrected for multiple comparisons with a false discovery rate (FDR) of 5%
164 (Benjamini and Hochberg, 1995). The BOLD response amplitudes were modeled for the
165 three (detection related) within-participant factors and compared them with a mixed-effects
166 meta-analysis (3dMEMA; Chen et al., 2012). We controlled for multiple comparisons with
167 family-wise error correction (see fMRI contrast analysis for details).

168

169 **Data and code availability**

170 The code to run the experiment, the behavioral data, and the code to analyze the
171 behavioral and MRI data are available at http://github.com/grundm/graphCA. Due to a lack
172 of consent of the participants, structural and functional MRI data cannot be shared
173 publicly, and can only be made available upon reasonable request if data privacy can be
174 guaranteed according to the rules of the European General Data Protection Regulation
175 (EU GDPR). The respective research group has to sign a data use agreement to follow
176 these rules. This statement is in line with our institute's policies and requirements by our
177 funding bodies.

178

179 **Behavioral paradigm**

180 Participants had both to report the perception (yes/no) of electrical pulses applied to their
181 left index finger and rate their confidence about their decision. Single square-wave pulses
182 (0.2 ms) were generated with a constant current stimulator (DS5; Digitimer, United
183 Kingdom) at individually assessed intensities near (mean intensity = 1.85 mA, range: 1.01-

3.48 mA) and supra (mean intensity = 2.18 mA, range: 1.19-3.89 mA) perceptual threshold reflecting 50% and 100% detection rate. Additionally, 25% of all trials were catch trials without stimulation.

Each trial (21 s) started with a fixation cross (1 s), followed by a cue (1 s) indicating an electrical pulse was soon to follow (Figure 1). The stimulation onset was always 100 ms before cue offset in order to temporally align the stimulation with the detection decisions. For aware trials participants' detection decisions presumably occur the instant the stimulation is noticed. However, for unaware trials they can only conclude there was no stimulus at cue offset. If the stimulus onsets had been pseudo-randomized across the cue window, the yes-decision would have occurred on average half of the cue window earlier than the no-decision. The actual reporting of the decision was delayed by 9 s to allow a movement-free time window for analyses. Participants had 1.5 s to report if they felt the stimulus or not by pressing the corresponding button for yes or no. Subsequently they had another 1.5 s to report their confidence about the yes/no-decision on a scale from 1 (very unconfident) to 4 (very confident). Any remaining time in the confidence rating window, following the rating, was added to a 7 s fixation cross creating an inter-trial interval of at least 7 s. Participants were instructed to place their right four fingers on a four-button box. The second and third buttons were controlled by the right middle finger and the ring finger to report the decision for yes or no. The outer buttons were controlled by the index finger and the little finger additionally to report the confidence decision on the full four-point scale. All button-response mappings were counterbalanced across participants. Hence depending on the mapping, the middle finger or the ring finger indicated "yes", and the four-point confidence scale started with "very confident" or "very unconfident" at the index finger.

Each block had in total 40 trials and lasted 14 min: 10 trials without stimulation, 25 with near-threshold intensity, and 5 with supra-threshold intensity, delivered in pseudo-

randomized order. Before each block, individual thresholds were assessed with an up-and-down method followed by the psi method from the Palamedes Toolbox (Kingdom and Prins, 2009). The threshold procedure followed that of the actual experimental trials but excluded the long pause and confidence response. Participants performed 4 blocks sequentially (circa 80 min). The experimental procedure was controlled by custom MATLAB scripts (The MathWorks Inc., Natick, Massachusetts) using Psychophysics Toolbox (Kleiner et al., 2007).

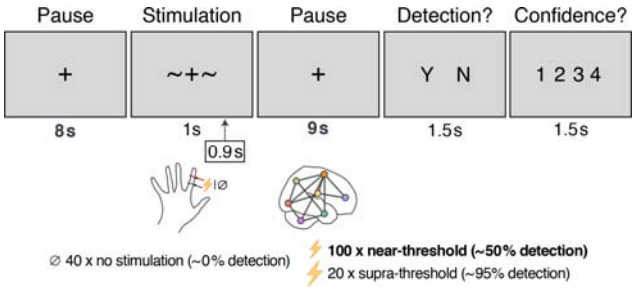

Figure 1. Experimental paradigm visualized across one trial (21 s). The tiles represent the participant's visual display and the times given below indicate the presentation duration. In total, each participant completed 160 trials across 4 blocks, including 100 near-threshold trials. Electrical nerve stimulation was applied to the left index finger 0.9 s after cue onset (~+~) to temporally align yes/no-decisions, which presumably had to be made at cue offset. Participants only reported their target detection decision (yes/no) following a long pause of 9 s in order to model the brain's post-stimulus functional network without a button press-related signal. The detection decision was followed by a confidence rating on a scale from 1 (very unconfident) to 4 (very confident). Every 0.75 s, a full MRI brain volume (BOLD) was acquired with a 3-mm isotropic resolution.

fMRI data acquisition

While participants performed the task, we acquired whole-brain BOLD contrast images with a 32-channel head coil on a Siemens MAGNETOM Prisma 3 Tesla scanner. For sub-second, whole-brain images, we used a Multi-Band (MB) echo-planar imaging (EPI)

sequence (Moeller et al., 2010; Setsompop et al., 2012) with an MB acceleration factor of 3 (TR = 750 ms, TE = 25 ms, flip angle = 55°, receiver bandwidth = 1815 Hz/px, partial Fourier = 7/8). No GRAPPA acceleration was applied (iPAT factor = 1). In each of the 4 blocks we acquired 1120 brain volumes (14 min), each consisting of 36 axial slices with a field of view of 192 x 192 mm² (64 x 64 voxel) and a 0.5-mm gap resulting in 3-mm isotropic voxels.

For magnetic distortion correction of the EPI scans, B0 images were obtained from double-echo GRE images (TR = 750 ms, TE_1 = 4.92 ms, ΔTE = 2.46 ms, echo spacing = 0.66 ms, flip angle = 45°), with the same voxel geometry as used for the EPI scans. The receiver bandwidth was 822 Hz/pixel.

For normalizing the EPI scans and extracting nuisance regressors of core white matter voxels and ventricles, we used previously acquired T1-sensitive brain images of the participants with a 32-channel head coil or for two participants with a 20-channel head/neck coil on 3-Tesla Siemens MAGNETOM Prisma, Skyra, TrioTim or Verio scanner. The MPRAGE sequence covered the whole brain (176 x 240 x 256 m^3) with an isotropic voxel resolution of 1 mm and slightly varied regarding the echo time and the receiver bandwidth across participants (TR = 2.3 s, TE = [2.01 (2), 2.96 (9), 2.98 (19), 4.21 (5)] ms, inversion time TI = 900 ms, flip angle = 9°, bandwidth = [238 (10), 240 (16), 241 (9)] Hz/px). For two participants, the sequence parameters were more different (TR = 1.3 s, TE = 3.5 ms, inversion time = 650 ms, flip angle = 8°/10°, bandwidth = 190 Hz/px).

Behavioral data analysis

The behavioral data was analyzed with R 3.6.0 in RStudio 1.2.1335. Data by four participants was incomplete due to technical issues and failed data acquisition. The blocks of the remaining 34 participants were evaluated for successful near-threshold assessments if at least 4 null and 17 near-threshold trails with a yes/no and confidence

response were recorded. This meant that only blocks with a hit rate at least 5 percentage points larger than the false alarm rate and participants with an average hit rate of 20-80% were further processed. This resulted in 31 participants with on average 89 near-threshold trials (range: 66-100). The distribution of mean detection rates is visualized in Figure 2a. For the confidence ratings, we calculated conditional probabilities for each confidence rating given a stimulus-response condition: correct rejection, near-threshold miss, near-threshold hit, and supra-threshold hit (Figure 2b). The conditional probabilities were compared with paired *t*-tests between neighboring conditions (correct rejection vs. near-miss, near-miss vs. near-hit, near-hit vs. supra-hit). The twelve *p*-values were FDR-corrected with a false discovery rate of 5% (Benjamini and Hochberg, 1995) and visualized with the means in Figure 2b.

fMRI preprocessing

Each EPI block was preprocessed with custom bash scripts using AFNI 18.2.17, FSL 5.0.11, and FreeSurfer 6.0.0 (Cox, 1996; Fischl, 2012; Smith et al., 2004). The code is available on http://github.com/grundm/graphCA. After removing the initial 10 volumes, the time series were despiked and corrected for slice timing. Subsequently, the volumes were corrected for motion and distortion using field maps acquired at the beginning of the experiment. We applied a non-linear normalization to MNI space (AFNI 3dQwarp). Next to the realignment to correct for motion, we calculated the euclidean norm (enorm) to censor volumes with large motion for the functional connectivity and BOLD contrast analyses. Volumes were ignored when they exceeded motion > 0.3 mm (enorm = sqrt(sum squares) of motion parameters; AFNI 1d_tool.py -censor_motion). Compared to the framewise displacement (FD = sum(abs) of motion parameters; Power et al., 2012), the euclidean norm has the advantage to represent appropriately large motion, e.g., the six parameters “6 0 0 0 0 0” and “1 1 1 1 1 1” would be the same for FD (FD = 6) in contrast to a enorm of

6 and 2.45, respectively. Modeling the functional connectivity and the BOLD contrasts was done with AFNI 19.1.05.

fMRI whole-brain contrast analysis

For the BOLD contrast analysis, the data was additionally smoothed with a 7-mm FWHM kernel and scaled to a mean of 100 and maximum of 200. In the final step, we calculated a nuisance regression to control for (a) motion with Friston's 24-parameter model (Friston et al., 1996), (b) signal outliers and their derivatives, (c) each 3 first principal components of core voxels in ventricle and white matter masks separately, and (d) a constant and trends up to polynomial of degree six (~high-pass filter > 0.0046 Hz) separately for each block.

We calculated an individual general linear model (GLM) for each participant with AFNI 3dREMLfit that combined all blocks and modeled the BOLD response as a gamma function for the following conditions: correct rejections, near-threshold misses, and near-threshold hits. A second model included confident correct rejections, confident misses, and confident hits (pooled confidence ratings of 3 and 4). Furthermore, two BOLD response regressors for the button presses of the yes/no-decision and the confidence rating were included. The regressors of the nuisance regression served as baseline regressors (AFNI 3dDeconvolve -ortvec).

The estimated regression coefficients for the aware and unaware condition were tested against each other with a mixed-effects meta-analysis (3dMEMA; Chen et al., 2012). This approach accounts for within-participant variability by using the corresponding *t*-statistics of the regression coefficients from each participant. Additionally, the detection rate was used as a covariate to account for the interindividual variance. The resulting volumes with *t*-values were corrected for multiple comparisons by thresholding voxels at $p_{voxel} < 0.0005$ and the resulting clusters at *k* voxels ($p_{cluster} = 0.05$). The cluster size threshold *k* was derived for each contrast separately based on 10,000 simulations without

a built-in math model for the spatial autocorrelation function as recommended by AFNI (for details see 3dttest++ with Clustsim option and Cox et al. (2017) as response to Eklund et al. (2016)). The rendered brain images were created with MRIcron (Rorden and Brett, 2000).

fMRI contrast analysis in primary somatosensory cortex

Furthermore, we wanted to evaluate the BOLD signal for the near-threshold stimulation in the primary somatosensory cortex. Unlike the fMRI contrast analysis for the whole brain described above, the BOLD data was not smoothed, scaled or part of a nuisance regression. We modeled the BOLD response for all near-threshold trials and trials without stimulation (independent of the yes/no-responses). The GLMs also included one regressor for each button press. The baseline regressors were limited to (a) Friston's 24-parameter model, (b) signal outliers and their derivatives, and (c) a constant and a linear trend separately for each block (polynomial of degree one). The estimated regression coefficients for the trials with and without near-threshold stimulation were compared with a mixed-effects meta-analysis (3dMEMA; Chen et al., 2012) that included the detection rate as a covariate. Additionally to reporting the contrast "stimulus present > absent" for the whole-brain, this analysis was limited to the right primary somatosensory cortex (Area 3b and Area 1) as defined by a multi-modal parcellation based brain atlas (Glasser et al., 2016).

Functional connectivity analysis

For estimating the context-dependent functional connectivity between regions of interest (ROI), we used the generalized psychophysiological interaction (gPPI; McLaren et al., 2012) without the deconvolution step, as implemented in FSL (O'Reilly et al., 2012). The deconvolution algorithm tries to estimate the underlying neural activity to match it

temporally with the psychological context (Cisler et al., 2014; Gitelman et al., 2003; McLaren et al., 2012). However, it cannot be determined if this estimate is correct (Cole et al., 2013; O'Reilly et al., 2012). Furthermore, also Godwin et al. (2015) repeated their analysis without the deconvolution step. Hence, we followed the FSL implementation and convolved the psychological variable with a fixed-shaped HRF to temporally align it with the measured BOLD signal (O'Reilly et al., 2012). The gPPI model included (a) regressors for the BOLD response function for each condition, (b) a regressor for the baseline functional connectivity of a seed region of interest (ROI), and (c) regressors for the context-dependent functional connectivity of the ROI for each condition (psychophysiological interaction). For (b), the seed ROI average time series was extracted to be used as a regressor. For (c), this baseline regressor was masked for each condition separately to generate conditional interaction regressors. The mask for each condition was equivalent to the regressor that modeled the BOLD response for the corresponding condition, hence weighting the seed time series in the post-stimulus phase with the hemodynamic response. The interaction regressors for each condition allowed the estimation of (c) the context-dependent functional connectivity by accounting for (a) the BOLD response and (b) the baseline functional connectivity (Figure 5b). Additionally, the gPPI included baseline regressors: (a) Friston's 24-parameter model for motion, (b) signal outliers and their derivatives, and (c) a constant and a linear trend separately for each block (polynomial of degree one).

The gPPI was calculated with AFNI 3dREMLfit for a whole-brain network of 264 nodes based on a resting-state functional connectivity atlas (Power et al., 2011). The nodes were defined as 4-mm radius, spherical ROIs at the atlas' MNI coordinates. The BOLD response model was a gamma function. AFNI 3dREMLfit has the advantage of allowing for serial correlations by estimating the temporal autocorrelation structure for each voxel separately.

For each node's gPPI, the coefficients of the context-dependent functional connectivity regressors were extracted from all other nodes separately by averaging across all voxels constituting the particular node. Subsequently, the beta values were combined in a symmetric connectivity matrix for each participant and each condition. As Godwin et al. (2015), we did not assume directionality and averaged the absolute values of reciprocal connections. Subsequently, the connectivity matrices were thresholded proportionally for the strongest connections and rescaled to the range [0,1] by dividing all values by the maximum value. The figures showing nodes and edges on a glass brain (Figure 5a,e) were created with BrainNet Viewer 1.6 (Xia et al., 2013).

After running the functional connectivity analysis as Godwin et al. (2015) for only confident trials, we repeated the analysis for all trials independent of their confidence response. Furthermore, we extended the preprocessing to include 7-mm smoothing, scaling and a nuisance regression and redid the analysis for both trial selections (confident only and all). For this analysis, the baseline regressors were (a) Friston's 24-parameter model, (b) signal outliers and their derivatives, (c) each three first principal components of core voxels in ventricle and white matter masks separately, and (d) separately for each block a constant and trends up to polynomial of degree six (~high-pass filter > 0.0046 Hz).

Graph-theoretical analysis

The context-dependent connectivity matrices were further processed with the Brain Connectivity Toolbox (BCT Version 2017-15-01; Rubinov and Sporns, 2010) to describe their network topologies. Across proportional thresholds (5-40%) graph metrics were calculated and normalized with the average graph metrics of 100 random networks with the same degree distribution (see BCT function randmio_und.m on https://sites.google.com/site/bctnet/Home/functions). In order to compare our results with the report for visual awareness (Godwin et al., 2015), we chose the same metrics for (a)

segregation, (b) integration, and (c) centrality: (a) weighted undirected modularity (BCT function modulartiy_und.m; Newman, 2004) and weighted undirected clustering coefficient averaged over all nodes (BCT function clustering_coef_wu.m; Onnela et al., 2005), (b) weighted characteristic path length (BCT function charpath.m), and (c) weighted participation coefficient averaged over all nodes (BCT function participation_coef.m; Guimerà and Nunes Amaral, 2005). The participants' graph metrics were compared between each condition with the Wilcoxon's signed-rank test because the distributions of the graph metrics are unknown. The resulting 24 *p*-values for each graph metric (8 network threshold times 3 comparisons: hit vs. miss, hit vs. correct rejection, and miss vs. correct rejection) were FDR-corrected with a false discovery rate of 5% (Benjamini and Hochberg, 1995). Furthermore, we calculated the Bayes factors based on *t*-tests with a JZS prior ($r = \sqrt{2}/2$) to assess the evidence for the null hypothesis (Rouder et al., 2012).

Results

Behavioral data

Participants (N = 31) detected on average 55% of the near-threshold pulses (SD = 13%), 88% of the supra-threshold pulses (SD = 12%), and correctly rejected 97% of the catch trials without stimulation (SD = 6.0%; Figure 2a). Participants reported on average to be "rather confident" or "very confident" for 87% of the correct rejections (SD = 13%), 70% of the near-threshold misses (SD = 23%), 59% of the near-threshold hits (SD = 27%) and 89% of the supra-threshold hits (SD = 13%). Participants reported significantly more often "very confident" for near-threshold misses (M = 37.2%) than hits (M = 28.7%, FDR-corrected p = 0.037) and less often "very unconfident" for misses (M = 6.9%) than hits (M = 17.7%, FDR-corrected p = 0.023; Figure 2b). The conditional probabilities for "rather unconfident" and "rather confident" did not differ between near-threshold hits and misses. Near-threshold misses and correct rejections differed in their conditional probabilities for "very unconfident", "rather unconfident" and "very confident" (Figure 2b) indicating higher confidence for correct rejections. Also, participants were on average more confident for supra-threshold hits than near-threshold hits. Additionally, we assessed the stability of near-threshold detection and false alarms across the experiment. We used linear mixed-effects models with maximum likelihood estimation (lmer function in R) to investigate the effect of block on near-threshold hit rate (near_yes) and false alarm rate (null_yes). Model comparison of the model "near_yes ~ block + (1|ID)" with the null model "near_yes ~ 1 + (1|ID)" resulted in no significant difference (χ^2 = 1.40, p = 0.24), indicating no effect of block on near-threshold hit rate. Also, for false alarms, the linear mixed-effects model "null_yes ~ block + (1|ID)" was not significantly different compared to the null model "null_yes ~ 1 + (1|ID)" (χ^2 = 1.41, p = 0.23). Therefore, we conclude that the behavioral performance is not affected by acclimatization or mental fatigue.

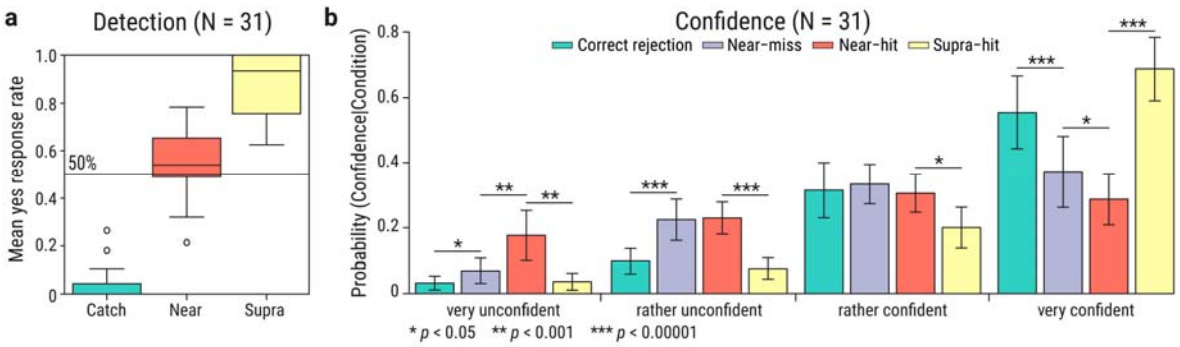

426

427 **Figure 2.** Mean detection rate and decision confidence across participants. (**a**) Detection rates for each trial
428 condition: without stimulation (catch trials) and with near- and supra-threshold stimulation. The central line
429 indicates the median in each box. The whiskers indicate 1.5 times the interquartile range or the maximum
430 value if smaller. Circles indicate values beyond this whisker range. (**b**) Mean conditional probabilities for
431 each confidence rating given a stimulus-response condition: correct rejection (green), near-threshold misses
432 (purple), near-threshold hits (red), and supra-threshold hits (yellow). Error bars indicate within-participants
433 95% confidence intervals (Morey, 2008). Horizontal lines indicate significant paired *t*-tests with FDR-
434 corrected *p*-values between neighboring conditions (Benjamini and Hochberg, 1995).

435 **BOLD amplitude contrasts**

436 First, we modeled the BOLD contrast between hits and misses (Figure 3a-c), as well as
437 misses and correct rejections independent of the confidence rating (Figure 3d-f). Second,
438 we compared only confident hits and misses (Figure 4a-c), as well as confident misses
439 and correct rejections (Figure 4d-f). Third, we modeled the contrast between near-
440 threshold stimuli and trials without stimulation for the whole brain (Figure 5) and the
441 primary somatosensory cortex only (Figure 6). The preprocessing for this contrast
442 excluded smoothing, scaling or nuisance regression. For all group-level comparisons, we
443 used the detection rate as a covariate to account for the interindividual variance (Figure
444 2a).

445 Contrasting near-threshold hits and misses (stimulus awareness) showed a fronto-
446 parietal network including the left inferior frontal gyrus (lIFG), the left nucleus accumbens
447 (lNAC), the left and right anterior insula (lINS1; rINS), the left and right intraparietal sulcus
448 (lIPS1; lIPS2; rIPS) and the right precuneus (rPCUN; Figure 3a-c, Table 1). When the
449 statistical threshold for the family-wise error was set to $p_{cluster} \leq 0.06$, resulting in a
450 decreased cluster size $k \geq 28$, two additional clusters were observed for hits compared to
451 misses in the contralateral secondary somatosensory cortex (cS2) and the left precuneus
452 (lPCUN). When comparing missed near-threshold trials with correctly rejected null trials
453 (somatosensory processing of undetected stimuli), the contra- and ipsilateral S2 (cS2b;
454 iS2), the left anterior insula (lINS2) and the left supplementary motor area (lSMA) showed
455 statistically significant activations (Figure 3d-f).

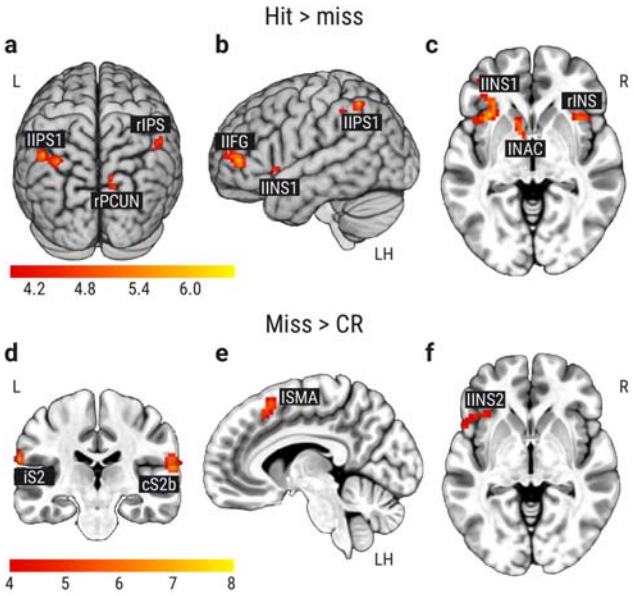

Figure 3. BOLD amplitude contrasts for awareness and stimulation effect. (**a-c**) Contrast between near-threshold hits and misses with focus on (**a**) the right precuneus (rPCUN) and the left and right intraparietal sulcus (lIPS1, rIPS1), (**b**) the left inferior frontal gyrus (lIFG) and (**c**) the left nucleus accumbens (lNAC) and the left and right anterior insula (lINS1, rINS; z = -3). Correction for multiple comparison with $t_{voxel}(30) \geq 3.92$, $p_{voxel} \leq 0.0005$ and cluster size $k \geq 31$ ($p_{cluster} \leq 0.05$). (**d-f**) Contrast between near-threshold misses and correct rejections (CR) of trials without stimulation. (**d**) Coronal view (y = -29) with the contralateral and ipsilateral secondary somatosensory cortices (cS2, iS2). (**e**) Sagittal view (x = -7) on the supplementary motor area (SMA). (**f**) Axial view (z = -3) on the left anterior insula (INS). Correction for multiple comparison with $t_{voxel}(30) \geq 3.92$, $p_{voxel} \leq 0.0005$ and cluster size $k \geq 27$ ($p_{cluster} \leq 0.05$). Left (L), right (R), and the left hemisphere (LH) are indicated.

Table 1. MNI coordinates for significant BOLD contrast clusters "hit > miss" and "miss > correct rejection (CR)" in Figure 3. Correction for multiple comparisons with $t_{voxel}(30) \geq 3.92$, $p_{voxel} \leq 0.0005$ and $p_{cluster} \leq 0.05$, resulting in a cluster size $k \geq 31$ for "hit > miss" and a cluster size $k \geq 27$ for "miss > CR". Clusters are ordered by volume (number of voxels). MNI coordinates of the maximum t value (peak) are reported in millimeters (mm) on the left-right (LR), posterior-anterior (PA) and inferior-superior (IS) axes. The mean t value is the average across all voxels of one cluster.

Contrast	Area	Label	Volume	LR	PA	IS	Mean
Hit > miss	Left anterior insula	lINS1	84	-35	19	-3	4.56
$p_{cluster} \leq 0.05 \mid k \geq 31$	Left intraparietal sulcus	lIPS1	74	-32	-62	50	4.50
$N = 31$	Right precuneus	rPCUN	64	13	-71	39	4.50
	Left nucleus accumbens	lNAC	62	-14	10	-10	4.47
	Left inferior frontal gyrus	lIFG	57	-44	46	4	4.54
	Right anterior insula	rINS	54	40	19	-7	4.56
	Right intraparietal sulcus	rIPS	42	52	-35	46	4.56
	Left intraparietal sulcus	lIPS2	37	-50	-41	46	4.21
$p_{cluster} \leq 0.06 \mid k \geq 28$	Right/contralateral S2	cS2a	30	58	-20	22	4.52
	Left precuneus	lPCUN	29	-11	-71	39	4.48
Miss > CR	Right/contralateral S2	cS2b	101	64	-20	14	4.78
$p_{cluster} \leq 0.05 \mid k \geq 27$	Left anterior insula	lINS2	75	-56	10	0	4.32
$N = 31$	Left/ipsilateral S2	iS2	52	-68	-26	22	4.73
	Left supplementary motor area	lSMA	32	-8	16	57	4.73

Second, we contrasted only confident hits, misses, and correct rejections. Trials were classified as confident when rated with 3 or 4 ("rather confident" or "very confident"). Since the first trial of each block was not considered for the fMRI analysis, the participants (N = 31) had on average 28 confident hits (SD = 14), 28 confident misses (SD = 15), and 29 confident correct rejections (SD = 7). For confident hits and misses, the precuneus bilaterally (PCUN), the left and the right intraparietal sulcus (lIPS, rIPS1, rIPS2), the posterior cingulate cortex (PCC) and the left anterior insula (lINS) had significant activation clusters with conscious tactile perception (Figure 4a-c). The contralateral secondary somatosensory cortex (cS2) showed activation again with the statistical threshold $p_{cluster} \leq 0.06$ (Table 2). Confident misses showed a higher activation than confident correct rejections in the ipsilateral and contralateral secondary somatosensory cortices (iS2, cS2). The cS2 cluster was reaching into the posterior insular cortex (Figure 4d-f).

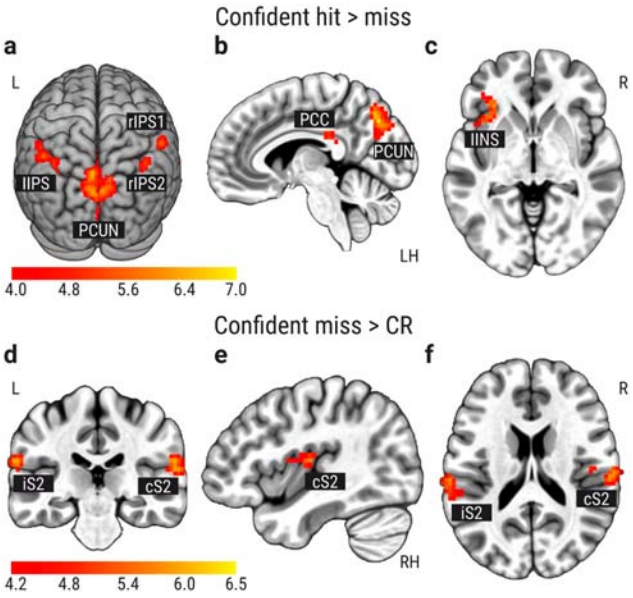

Figure 4. BOLD amplitude contrasts for only confident trials. Correction for multiple comparison with $t_{voxel}(30) \geq 3.92$, $p_{voxel} \leq 0.0005$ and cluster size $k \geq 28$ ($p_{cluster} \leq 0.05$). (**a-c**) Contrast between confident near-threshold hits and misses with focus on (**a**) the precuneus (PCUN) and the intraparietal sulcus (IPS), (**b**) the posterior cingulate cortex (PCC; x = -7), and (**c**) the left anterior insula (lINS; z = -3). (**d-f**) Contrast between near-threshold misses and correct rejections (CR) of trials without stimulation. (**d**) Coronal view (y = -26) with the contralateral and ipsilateral secondary somatosensory cortices (cS2; iS2). (**e**) Sagittal view (x = 41) on the cS2 cluster reaching into insular cortex. (**f**) Axial view on cS2 and iS2 (z = 18). Left (L), right (R), the left hemisphere (LH), and the right hemisphere (RH) are indicated.

Table 2. MNI coordinates for significant BOLD contrast clusters "confident hit > miss" and "confident miss > correct rejection (CR)" in Figure 4. Correction for multiple comparisons with $t_{voxel}(30) \geq 3.92$, $p_{voxel} \leq 0.0005$ and $p_{cluster} \leq 0.05$, resulting in a cluster size $k \geq 28$. Clusters are ordered by volume (number of voxels). MNI coordinates of the maximum *t* value (peak) are reported in millimeters (mm) on the left-right (LR), posterior-anterior (PA) and inferior-superior (IS) axes. The mean *t* value is the average across all voxels of one cluster.

Contrast	Area	Label	Volume	LR	PA	IS	Mean
Confident hit > miss	Left/right precuneus	PCUN	387	-8	-74	39	4.66
$p_{cluster} \leq 0.05 \mid k \geq 28$	Left intraparietal sulcus	lIPS	137	-47	-53	50	4.43
$N = 31$	Left anterior insula	lINS	57	-32	28	-3	4.68
	Right intraparietal sulcus	rIPS1	42	55	-38	50	4.46
	Posterior cingulate cortex	PCC	39	4	-35	22	4.45
	Right intraparietal sulcus	rIPS2	34	40	-62	53	4.33
$p_{cluster} \leq 0.06 \mid k \geq 26$	Right/contralateral S2	cS2	26	61	-20	22	4.36
Confident miss > CR	Right/contralateral S2	cS2	141	64	-20	14	4.56
$p_{cluster} \leq 0.05 \mid k \geq 28$	Left/ipsilateral S2	iS2	85	-65	-26	22	4.60

Third, we contrasted all near-threshold and catch trials independent of their behavioral response to investigate the stimulation effect in the whole brain. In contrast to the BOLD contrast analysis above, the preprocessing excluded smoothing, scaling or nuisance regression to align it with the preprocessing of the functional connectivity analysis. For the near-threshold stimulation compared to no stimulation, the ipsilateral and contralateral secondary somatosensory (iS2, cS2), the left anterior insula (lINS) and the right anterior cingulate cortex (rACC) showed significant clusters with a larger activation (Figure 5, Table 3).

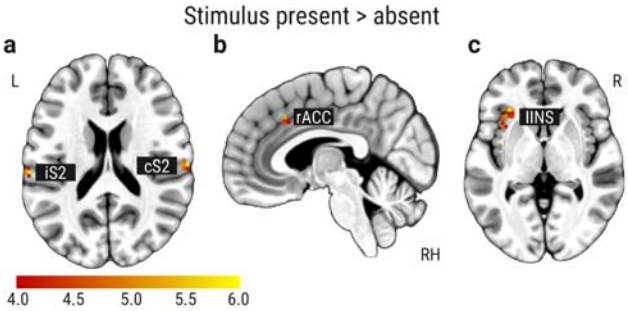

Figure 5. BOLD amplitude contrast for near-threshold stimulation. Correction for multiple comparison with $t_{voxel}(30) \geq 3.92$, $p_{voxel} \leq 0.0005$ and cluster size $k \geq 5$ ($p_{cluster} \leq 0.05$). (**a-c**) Contrast between near-threshold stimulation trials and trials without stimulation with significant clusters in (**a**) the ipsilateral and contralateral secondary somatosensory cortex (iS2, cS2; $z = 19$), (**b**) the right anterior cingulate cortex (rACC; $x = 4$), and (**c**) the left anterior insula (lINS; $z = 0$). Left (L), right (R), and the right hemisphere (RH) are indicated.

Table 3. MNI coordinates for significant BOLD contrast clusters "near-threshold stimulation > trials without stimulation (catch trials)" in Figure 5. Correction for multiple comparisons with $t_{voxel}(30) \geq 3.92$, $p_{voxel} \leq 0.0005$ and $p_{cluster} \leq 0.05$, resulting in a cluster size $k \geq 5$. Clusters are ordered by volume (number of voxels). MNI coordinates of the maximum *t* value (peak) are reported in millimeters (mm) on the left-right (LR), posterior-anterior (PA) and inferior-superior (IS) axes. The mean *t* value is the average across all voxels of one cluster.

Contrast	Area	Label	Volume	LR	PA	IS	Mean
Near > catch trials	Left anterior insula	lINS	35	-35	13	4	4.64
$p_{cluster} \leq 0.05 \mid k \geq 5$	Right anterior cingulate cortex	rACC	15	4	22	39	4.37
$N = 31$	Right/contralateral S2	cS2	13	64	-20	18	5.07
	Left/ipsilateral S2	iS2	6	-65	-26	18	4.62

Fourth, we contrasted all near-threshold and catch trials independent of their behavioral response only within the right primary somatosensory cortex (Area 3b and Area 1). The region of interest was defined by a multi-modal brain atlas (Glasser et al., 2016). Furthermore, the preprocessing did not include smoothing, scaling, or nuisance regression. We found positive and negative significant voxels for uncorrected $p_{voxel} \leq 0.05$ in Area 3b and Area 1. A positive voxel in the latter (x = 38, y = -38, z = 67; Figure 6) was close to previously reported peak coordinates in Area 1 (x = 38, y = -40, z = 66) for electrical stimulation of the median nerve (Schröder et al., 2019). Yet, these voxels did not meet the criteria by a correction for multiple comparisons (FDR-corrected $p \leq 0.05$ or a cluster size $k \geq 12$ for $p_{cluster} \leq 0.05$; Table 4). Additionally, a contrast of supra-threshold hits and correct rejections corrected for multiple comparisons in the whole brain ($p_{voxel} <$ 0.0005 and cluster size $k \geq 5$, $p_{cluster} \leq 0.05$) revealed a cluster in the contralateral primary somatosensory cortex (k = 6 voxels, mean t = 4.27) whose peak coordinates (x = 52, y = -32, z = 53) were in Area 1 according to the Eickhoff-Zilles atlas (Eickhoff et al., 2005).

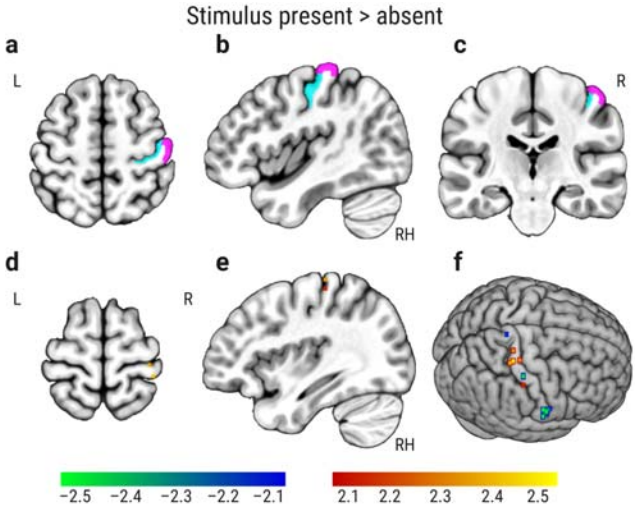

Figure 6. BOLD amplitude contrast for near-threshold stimulation in the primary somatosensory cortex (Area 3b and Area 1). (**a-c**) Region of interest Area 3b (cyan) and Area 1 (violet, z = 56, x = 43, y = -22). (**d-f**) Only voxels with $t_{voxel}(30) \leq -2.045$ and $t_{voxel}(30) \geq 2.045$, $p_{voxel} \leq 0.05$ (z = 68, x = 36). Left (L), right (R), and the right hemisphere (RH) are indicated.

Table 4. MNI coordinates for BOLD contrast clusters in the primary somatosensory cortex (Area 3b and Area 1) for "near-threshold stimulation > trials without stimulation (catch trials)" in Figure 6. Voxel threshold $t_{voxel}(30) \geq 2.045$ and $t_{voxel}(30) \leq -2.045$, $p_{voxel} \leq 0.05$ and cluster size $k \geq 2$. Clusters are ordered by displaying first the positive cluster and then the negative cluster. MNI coordinates of the maximum *t* value (peak) are reported in millimeters (mm) on the left-right (LR), posterior-anterior (PA) and inferior-superior (IS) axes. The mean *t* value is the average across all voxels of one cluster.

Contrast	Area	Label	Volume	LR	PA	IS	Mean
Near > catch trials	Right/contralateral Area 3b	A3b	2	31	-29	60	2.25
Near < catch trials	Right/contralateral Area 1	A1	7	67	-8	22	-2.63

Context-Dependent Graph Measures

We assessed whether tactile conscious perception is accompanied by alterations of the brain's functional network topology. An atlas of 264 nodes (Power et al., 2011) was used to capture the whole-brain network as in (Godwin et al., 2015), who reported decreased modularity and increased participation with visual awareness. Whole-brain functional networks were modeled for each condition with the generalized psychophysiological interaction (gPPI; McLaren et al., 2012) without the deconvolution step (O'Reilly et al., 2012); see Methods Functional Connectivity Analysis for details). The gPPI has the advantage of controlling the context-dependent functional connectivity estimates for (a) the stimulation-related BOLD response and (b) the baseline functional connectivity across the experiment (Figure 7b). The graph-theoretical analysis of the context-dependent functional connectivity matrices was performed with the Brain Connectivity Toolbox (Rubinov and Sporns, 2010) to test for changes in the same measures of integration and segregation as in (Godwin et al., 2015). We thresholded the context-dependent connectivity matrices across a range of proportional thresholds from 5% to 40% in steps of 5% (Garrison et al., 2015) and separately calculated their normalized modularity, mean clustering coefficient, mean participation coefficient and characteristic path length (Figure 7c-f). Since Godwin et al. (2015) analyzed the graph-theoretical metrics only for confident hits and misses, we first ran the analysis for confident trials only (Figure 8). Trials were classified as confident when the yes/no-decision was rated with 3 or 4 ("rather confident" or "very confident"). Additionally, we repeated the analysis for all trials independent of their confidence rating (Figure 10) and with an extended preprocessing including a nuisance regression (Figure 11, 12).

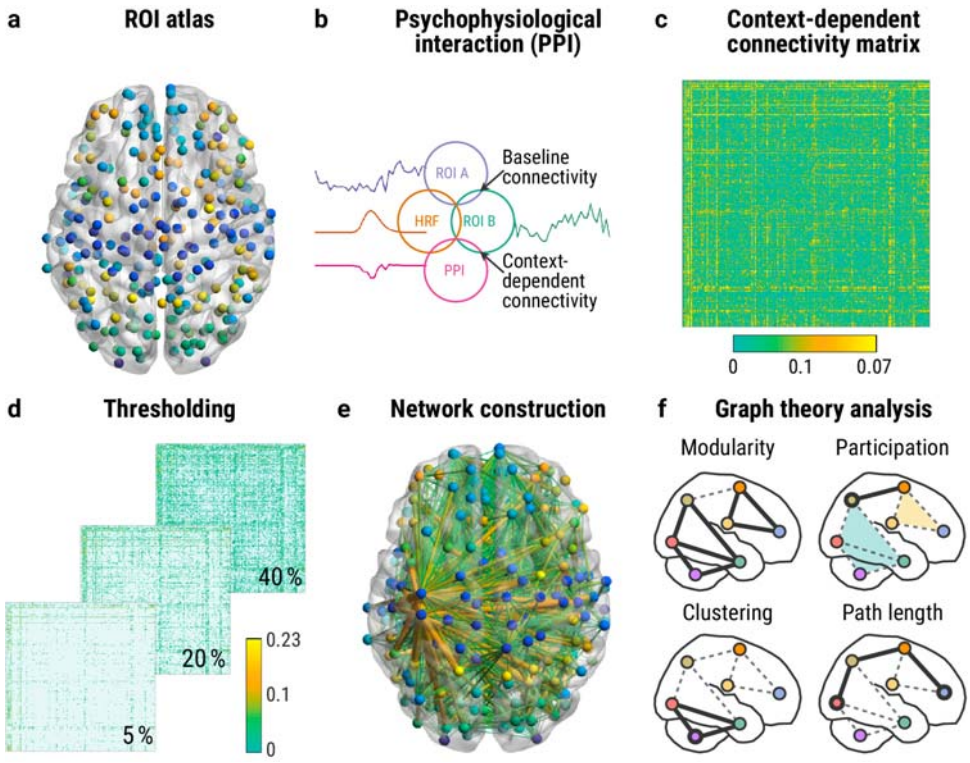

Figure 7. Context-dependent functional connectivity analysis. (**a**) Regions of interest (ROIs) were defined as 4-mm radius spheres at the MNI coordinates of a 264-nodes atlas (Power et al., 2011). (**b**) We used the generalized psychophysiological interaction (gPPI; McLaren et al., 2012) to calculate the context-dependent functional connectivity between all pairs of ROIs for each condition separately (hit, miss, and correct rejection). This measure controls for baseline functional connectivity and the stimulus-evoked hemodynamic response (HRF). (**c**) These context-dependent functional connectivity estimates were merged into individual, normalized, symmetric functional connectivity matrices to evaluate their network topology. For the latter, the matrices were thresholded to include only the strongest edges (**d**), and the resulting networks (**e**) were analyzed with graph-theoretical measures (**f**). For visualization, we selected the mean context-dependent connectivity matrix for hits (**c**) and thresholded it proportionally with 5-40% (**d**) and with 5% for the visualization of the edges (**e**). Edge color and diameter capture the strength of functional connectivity. Figure concept was inspired by Figure 2 in (Uehara et al., 2014).

Confident hits and misses showed no significant differences in measures of global segregation into distinct networks (modularity), local segregation (clustering), integration (path length), and centrality (participation) based on paired two-sided Wilcoxon's signed-rank tests and FDR-correction (Figure 8a-d). Additionally, we calculated the Bayes factors

based on paired *t*-tests with a JZS prior ($r = \sqrt{2}/2$; Rouder et al., 2012) to evaluate the evidence for the null hypothesis (H_0: confident hits and misses do not differ). For modularity, participation, clustering, and path length, the evidence was anecdotal or moderate for the null hypothesis across the network thresholds (Figure 8e-h). The Bayes factor for modularity was below 1 at the 10%-, 25%- and 30%-threshold (Figure 8e) and hence reflecting anecdotal evidence for the alternative hypothesis. Path length had a Bayes factor below 1 at the 20%-threshold (Figure 8h). Confident correct rejections showed no significant differences to confident misses or confident hits (Figure 8a-d). Furthermore, we calculated the mean connectivity matrices of each condition for the 10%-network threshold to visualize the context-dependent functional connectivity estimates across all 264 nodes (Figure 9).

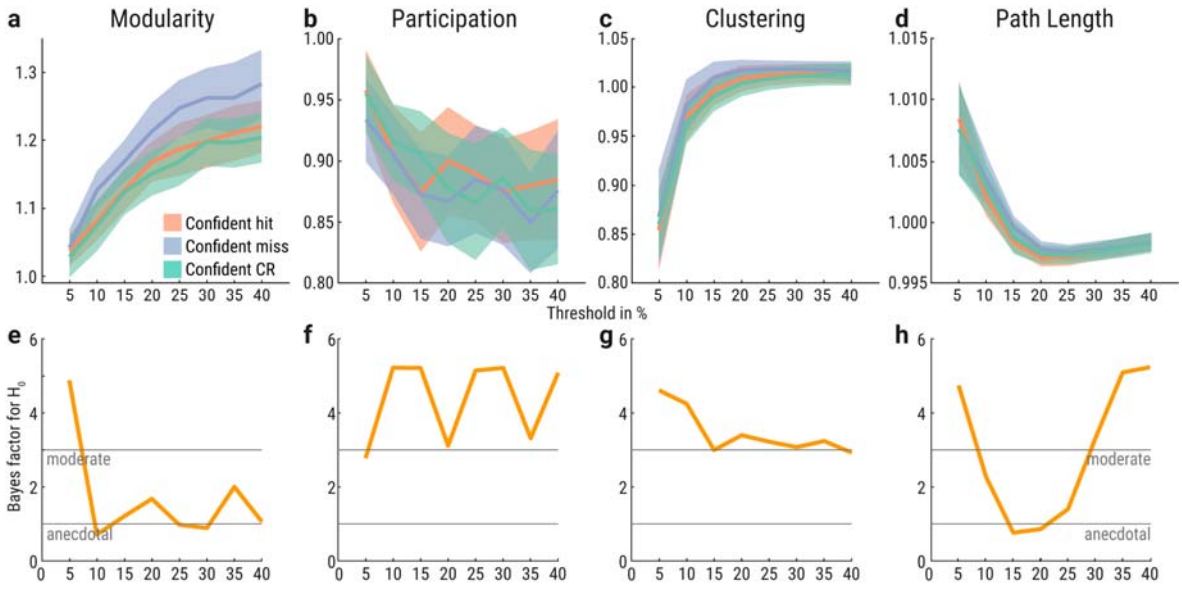

Figure 8. Functional network topology of only confident hits (red), misses (purple), and correct rejections (green). (**a-d**) Graph measures for network thresholds from 5-40% in 5% steps (x-axes). Y-axes indicate normalized graph metric values. Confidence bands reflect within-participant 95% confidence intervals. (**e-h**) Bayes factors (BF_{01}) based on paired *t*-test between confident hits and misses. Bayes factor of 2 indicates that the evidence for the null hypothesis is twice as likely compared to the alternative hypothesis given the data. Bayes factors between 1-3 are interpreted as anecdotal and between 3-10 as moderate evidence for the null hypothesis (Schönbrodt and Wagenmakers, 2018).

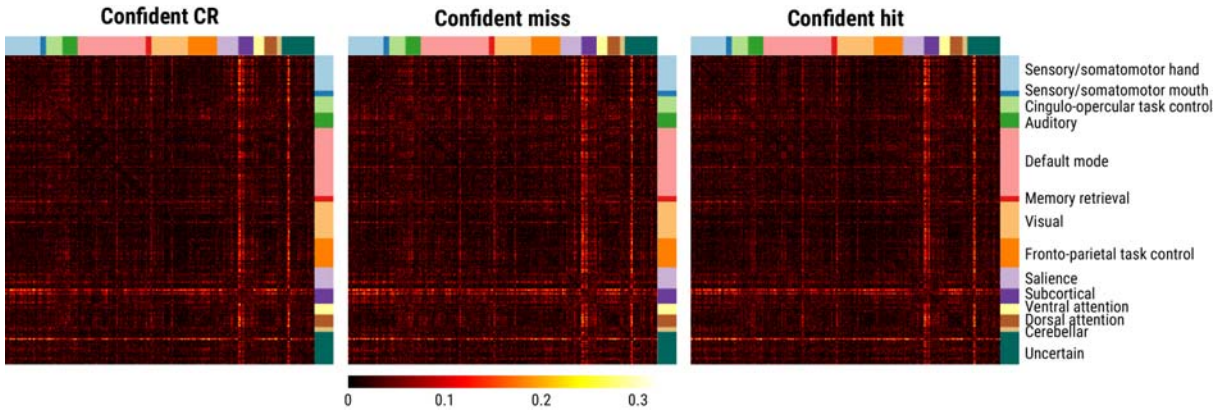

Figure 9. Mean connectivity matrices of confident correct rejections (CR), misses and hits for the 10%-threshold (Figure 8). The values represent the normalized gPPI estimates between the 264 nodes ordered by subnetworks.

Because graph metrics of the whole brain might be similar between conditions while the graph metrics of individual nodes and subnetworks differ, we normalized the averaged participation and clustering coefficients separately for each of the 14 Power et al. (2011) subnetworks. For this analysis, we chose the networks thresholded for the top 10% connections (Figure 9). The resulting graph metrics were compared with Wilcoxon's signed-rank tests between the three conditions while correcting for multiple comparisons with a false discovery rate of 5%. There was no significant difference in any subnetwork between confident correct rejections, misses, and hits.

We repeated the analysis for all trials independent of the confidence rating to increase the number of trials and hence the statistical power. As in the preceding analysis (Figure 8), we observed no significant differences in modularity, participation, clustering, and path length based on paired two-sided Wilcoxon's signed-rank tests and FDR-correction (Figure 10a-d). There was anecdotal to moderate evidence for the null hypothesis (H_0: hits and misses do not differ; Fig 9e-h). Only the Bayes factors for participation at the 40%-threshold (Figure 10f) and path length at the 20%-threshold (Figure 10h) were below 1 and hence reflected anecdotal evidence for the alternative hypothesis. Correct rejections showed no significant differences to misses or hits (Figure 10a-d).

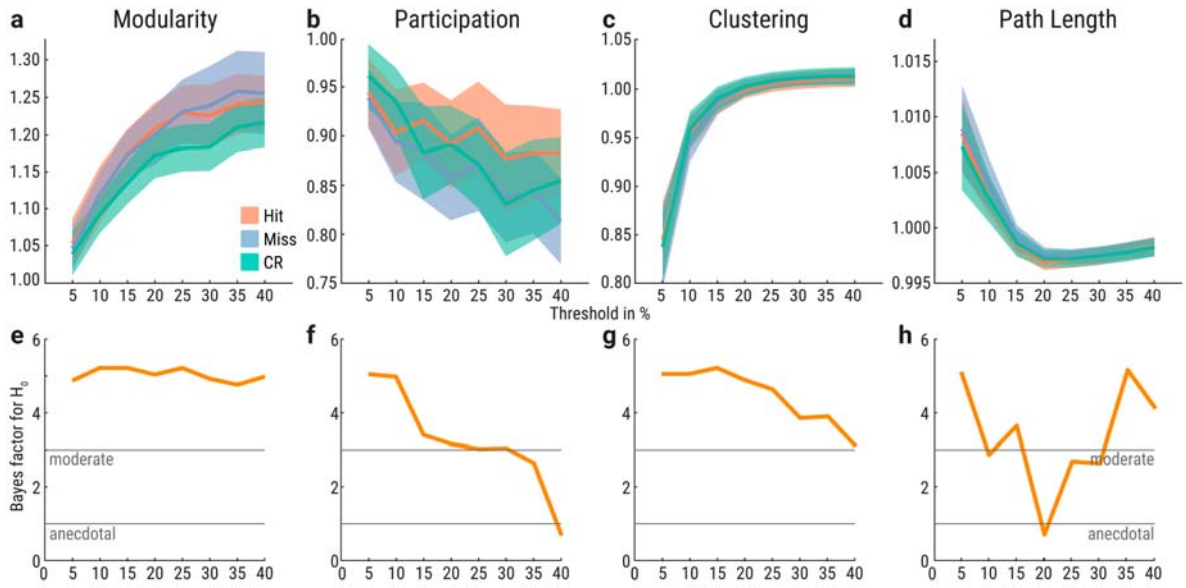

Figure 10. Functional network topology of all hits (red), misses (purple), and correct rejections (green). (**a-d**) Graph measures for network thresholds from 5-40% in 5% steps (x-axes). Y-axes indicate normalized graph metric values. Confidence bands reflect within-participant 95% confidence intervals. (**e-h**) Bayes factors (BF_{01}) based on paired *t*-tests between detected and undetected near-threshold trials. Bayes factor of 2 indicates that the evidence for the null hypothesis is twice as likely compared to the alternative hypothesis given the data. Bayes factors between 1-3 are interpreted as anecdotal and between 3-10 as moderate evidence for the null hypothesis (Schönbrodt and Wagenmakers, 2018).

In a third step, we extended the preprocessing to include smoothing, scaling and a nuisance regression as in the whole-brain BOLD contrast analysis (Figure 3, 4). We then analyzed again the graph metrics for only confident trials (Figure 11) and all trials independent of the confidence response (Figure 12). For only confident trials, we observed no significant differences in modularity, participation, clustering, and path length based on paired two-sided Wilcoxon's signed-rank tests and FDR-correction (Figure 11a-d). There was anecdotal to moderate evidence for the null hypothesis (H_0: confident hits and misses do not differ; Figure 8e-h). Confident correct rejections showed no significant differences to confident misses or confident hits (Figure 11a-d).

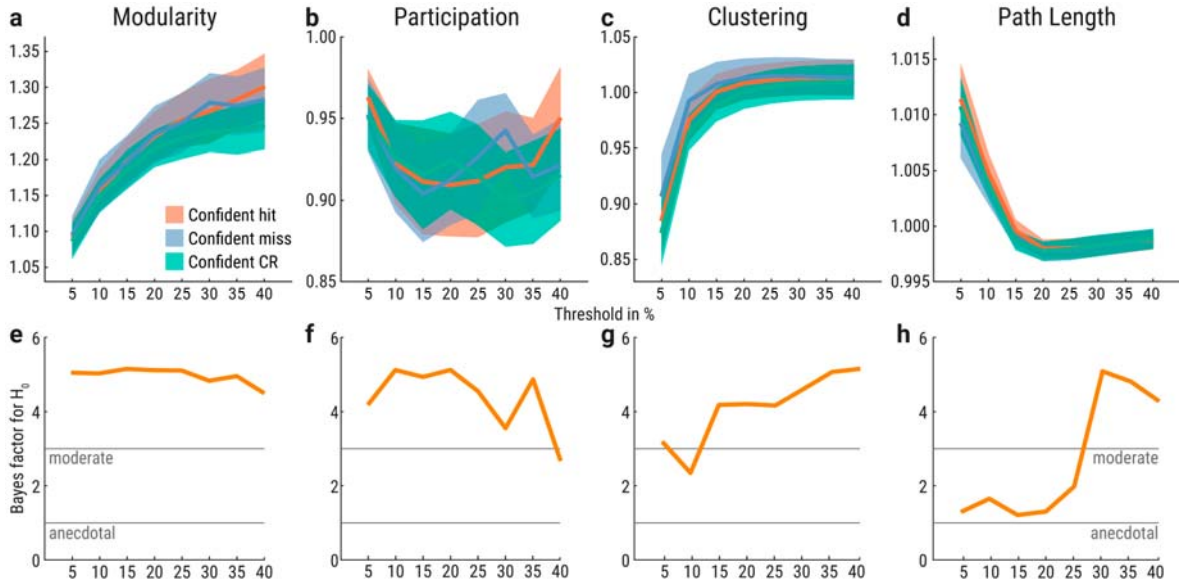

Figure 11. Functional network topology of only confident hits (red), misses (purple), and correct rejections (green) with extended preprocessing. (**a-d**) Graph measures for network thresholds from 5-40% in 5% steps (x-axes). Y-axes indicate normalized graph metric values. Confidence bands reflect within-participant 95% confidence intervals. (**e-h**) Bayes factors (BF_{01}) based on paired *t*-tests between confident detected and undetected near-threshold trials. Bayes factor of 2 indicates that the evidence for the null hypothesis is twice as likely compared to the alternative hypothesis given the data. Bayes factors between 1-3 are interpreted as anecdotal and between 3-10 as moderate evidence for the null hypothesis (Schönbrodt and Wagenmakers, 2018).

For the extended preprocessing and all trials independent of the confidence response, hits and misses did not differ significantly in modularity, participation, clustering, and path length based on paired two-sided Wilcoxon's signed-rank tests and FDR-correction (Figure 12a-d). There was anecdotal or moderate evidence for the null hypothesis (H_0: hits and misses do not differ; Figure 12e-h). Only the Bayes factors for path length at the 10%- and 15%-threshold were below 1 (Figure 12h) and hence reflected anecdotal evidence for the alternative hypothesis. The path length was higher for correct rejections than hits at the 35%-threshold (FDR-corrected p = 0.017), and at the 40%-threshold (FDR-corrected p = 0.042).

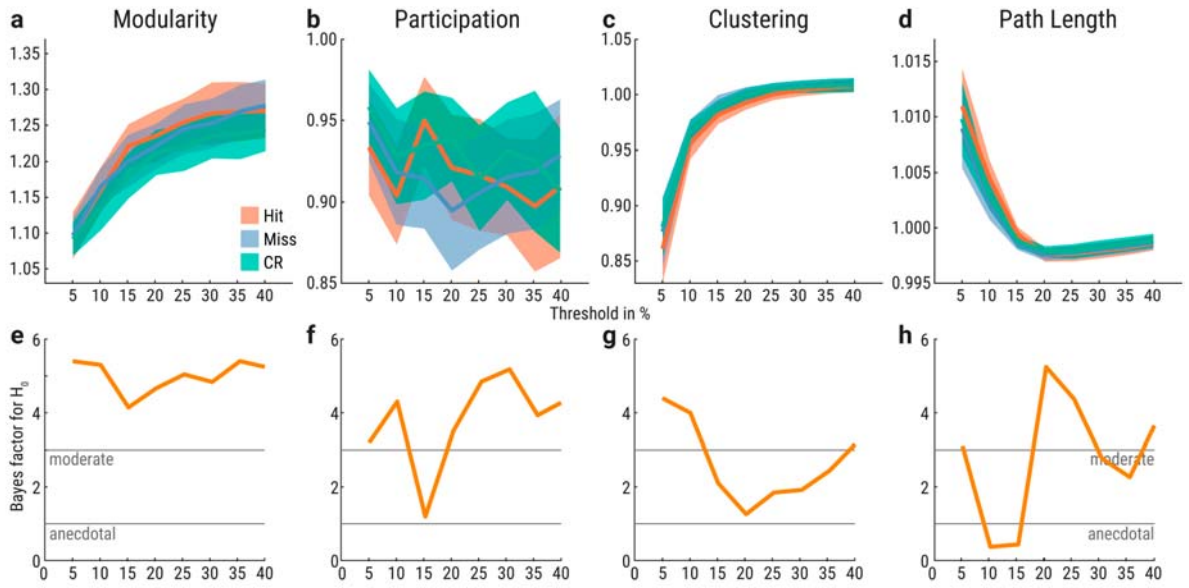

Figure 12. Functional network topology of all hits (red), misses (purple), and correct rejections (green) with extended preprocessing. (**a-d**) Graph measures for network thresholds from 5-40% in 5% steps (x-axes). Y-axes indicate normalized graph metric values. Confidence bands reflect within-participant 95% confidence intervals. (**e-h**) Bayes factors (BF_{01}) based on paired *t*-tests between detected and undetected near-threshold trials. Bayes factor of 2 indicates that the evidence for the null hypothesis is twice as likely compared to the alternative hypothesis given the data. Bayes factors between 1-3 are interpreted as anecdotal and between 3-10 as moderate evidence for the null hypothesis (Schönbrodt and Wagenmakers, 2018).

Furthermore, to investigate whether the atlas-based approach missed functional connectivity of subnetworks, we performed a seed-based gPPI analysis with the cS2 cluster from the contrast between near-threshold and catch trials (Figure 5; x = 64, y = -20, z = 18). We created a 4-mm radius sphere and extracted the mean BOLD time course, as in the atlas-based approach. After computing individual gPPI models, we tested the psychophysiological interaction regressors of the three conditions (confident correct rejections, misses, and hits) against each other across participants for all voxels and applied a cluster correction for multiple comparisons ($p_{voxel} \leq 0.0005$, cluster size $k \geq 4$ for $p_{cluster} \leq 0.05$). We did not observe any significant cluster for the cS2 functional connectivity contrast between confident hits and misses, and confident hits and correct rejections. For the contrast of confident misses and correct rejections, we found one negative significant cluster at threshold (cluster size k = 4 voxels) in the right cerebellum (x = 7, y = -41, z = 17). We repeated the analysis with extended preprocessing (including smoothing, scaling, and nuisance regression) and with all trials independent of their confidence response (corresponding to Figure 11). We did not observe any significant cluster for the cS2 functional connectivity contrast between any two of the three conditions (correct rejections, misses, and hits) for $p_{voxel} \leq 0.0005$ and $p_{cluster} \leq 0.05$ (cluster size $k \geq 18$ for hits vs. misses, and cluster size $k \geq 19$ for hits vs. correct rejections, and misses vs. correct rejections). That is why we conclude that the small negative cluster between confident misses and correct rejections is a spurious finding.

Discussion

Using fMRI during a near-threshold somatosensory detection task, we investigated changes in local brain activity and functional brain network topology associated with conscious perception. We found that conscious somatosensory perception ('detected' compared to 'undetected' stimuli) led to higher activation in precuneus, intraparietal sulcus, insula, inferior frontal gyrus, and nucleus accumbens. The latter two showed higher activation only when all trials were included (confident and unconfident) but not with confident trials only. At a slightly looser statistical threshold (p = 0.06) bilateral secondary somatosensory cortex also showed higher activity during conscious perception. Significant positive voxels in contralateral S1 for near-threshold stimuli were only noted in an ROI-based analysis. The graph-theoretical analysis of network topology did not provide any evidence for a difference between aware and unaware trials in modularity, participation, clustering, nor path length. Finally, when comparing misses with correctly rejected catch trials, we found activation of S2, insula, and supplementary area; also, in this contrast, no changes in network properties were observed. Subsequently, we first discuss the observed BOLD activity patterns and then the absent graph metric changes in comparison to the findings in the visual system using a masking paradigm by Godwin et al. (2015).

It is generally accepted, that primary and secondary somatosensory cortices (S1, S2) are necessary for somatosensory processing leading to conscious perception (Hirvonen and Palva, 2016; Moore et al., 2013). It has long been established that lesions in S1 go along with hypoesthesia (Roland, 1987). Recently, we have shown in stroke patients, that - despite intact S1 - also lesions in S2 (along with anterior and posterior insula, putamen, and subcortical white matter connections to prefrontal structures) lead to impaired tactile conscious experience (Preusser et al., 2015). fMRI studies employing supra-threshold somatosensory stimulation - in passive or active designs - have consistently shown activation of S1 and S2 (Ruben et al., 2001). As we have previously

shown, S1 and S2 are already affected by subthreshold stimuli (below the absolute detection threshold), which lead to a deactivation of these areas (Blankenburg et al., 2003). In the current study, we now show that near-threshold stimuli, which are not detected, i.e., below the response criterion (in signal detection theory terminology) for conscious detection, lead to an activation of S2 and insula (when compared to 'correct rejections' of catch trials). This leads to the interesting conclusion that non-detected stimuli lead to differential involvement of S1 and S2 depending on their intensity. Similarly, in our recent EEG study, we found that non-detected stimuli lead to a negativity 150 milliseconds after stimulation (N150) for principally detectable near-threshold stimuli but not for imperceptible stimuli intensities (Forschack et al., 2020). The N150 has been shown to originate in area S2 (Auksztulewicz et al., 2012). It will be an interesting issue for future studies whether an analysis based on objective detection paradigms (e.g., two-alternative forced-choice tasks, 2AFC) will further help to differentiate the meaning of these signal changes in S1 and S2, i.e., whether the "transition" from deactivation in S2 (and S1) to an activation is related to the "objective detection" in a criterion-free 2AFC task and the emergence of the N150. It should be noted that while others have shown that S1 represents the stimulus properties that get access to consciousness in interaction with S2 (Blankenburg et al., 2006; Moore et al., 2013; Rajaei et al., 2018; Schröder et al., 2019), we did not observe a strong stimulation effect in S1 for our near-threshold trials. This might be due to the weak stimulus intensity and stimulation "only" at the index finger in contrast to the commonly used median nerve stimulation.

For theories of consciousness, the difference between perceived versus non-perceived stimuli is most relevant. In our study, contralateral secondary somatosensory cortex (cS2) was found for both contrasts "hit > miss" and "confident hit > miss" when the statistical cluster threshold was set to $p = 0.06$. This finding is consistent with previous suggestions that there is additional activity in S2 with conscious detection. For example, a

748 previous fMRI study on vibrotactile detection reported ipsilateral and contralateral S2 as
749 the best correlate for detection success (Moore et al., 2013), and in another recent study
750 bilateral S2 activity was best explained by a psychometric (detection) function (Schröder et
751 al., 2019). One reason for detection-associated S2 activity might be recurrent processing
752 (Lamme, 2006; van Gaal and Lamme, 2012). For example, in an EEG study, the detection
753 of near-threshold electrical pulses to the finger was best explained by the recurrent
754 processing between contralateral S1 and S2, as well as contralateral and ipsilateral S2
755 (Auksztulewicz et al., 2012). Another explanation might be that separate parts of the
756 secondary somatosensory cortex might serve different functions. E.g., in a recent study,
757 more inferior and superior parts of cS2 correlated with a binary detection function, and
758 more posterior and anterior parts of cS2 correlated with a linear intensity function
759 (Schröder et al., 2019).

760 While our data overall agree with the necessity of S1 and S2 activation for
761 conscious perception, it is less clear whether activation of these areas is sufficient for
762 conscious somatosensory perception: The fact that certain areas “best explain” detection
763 in an fMRI study (Schröder et al., 2019), does not rule out that the activity of other areas is
764 also involved in the conscious experience. Like several previous studies on conscious
765 perception in other sensory domains (Bisenius et al., 2015; Dehaene and Changeux,
766 2011; Naghavi and Nyberg, 2005; Rees et al., 2002), we find fronto-parietal areas more
767 active in the ‘detected versus missed’ contrast. Among these, the activations in left and
768 right intraparietal sulcus, the bilateral posterior cingulate cortices, and the bilateral
769 precuneus are consistent with the notion of a “posterior hot zone” for conscious
770 experience as suggested by Koch and colleagues (Koch et al., 2016). Koch et al. (2016)
771 argue that the increased activity that is seen with conscious perception in additional (e.g.,
772 frontal) brain areas is related to response preparation, and/or other task-related activations
773 (confidence, etc.) as they have not been found activated in a no-response paradigm

(Frässle et al., 2014). For example, in our study, the nine-second period between stimulation and response most likely leads to increased activity in areas involved in working memory (see, e.g., tactospatial sketchpad, Schmidt and Blankenburg, 2018). Recent literature has pointed out this interrelation: the default mode network (e.g., posterior cingulate cortex) supports a stronger global workspace configuration, which improves working memory performance (Vatansever et al., 2015) and might be beneficial for conscious perception. On the other hand, even if one assumes that a "pure sensory conscious experience" could arise from a "posterior hot zone" only, the increased activity in other brain areas with conscious perception - still leaves the possibility of conscious experience related to action, confidence, working memory etc. to be dependent on e.g., frontal brain areas (Frith, 2019). In this view, the "integrated conscious experience" during a task would then be related to the entire fronto-parietal network. Obviously, this notion is close to the global workspace theory (Dehaene et al., 2006; Dehaene and Changeux, 2011; Mashour et al., 2020). While our data do not allow to definitely differentiate between these major theories of consciousness, we provide new information for somatosensory conscious perception, which is consistent with the idea that domain-general areas (interacting with domain-specific areas for example via recurrent processing (Lamme, 2006; van Gaal and Lamme, 2012) play a role for conscious perception.

A major hypothesis underlying our study was that conscious perception goes along with widespread changes in graph metrics as it has recently been reported by Godwin et al. (2015) for the visual system. However, we did not observe such context-dependent functional connectivity changes that result in network topology alterations through modularity, participation, clustering and path length between hits, misses or correct rejections. This does not change when the number of trials is increased by considering all trials independent of their confidence response (Figure 10). Also, improving the preprocessing with a nuisance regression that controls for motion and noise components

derived from white matter and ventricles, does not affect this result (Figure 11, 12). The isolated network topology differences between correct rejections and hits at the 35-40%-threshold for path length with the improved preprocessing (Figure 12d) were not consistent across thresholds and not present in the analysis of only confident trials (Figure 11), as well as in the analyses with the basic preprocessing (Figure 8, 10). That is why we do not interpret these differences as a valid and reliable effect. Thus, there was neither a functional network alteration by stimulus awareness (hit > miss) nor by the detected (hit > CR) or undetected stimulation (miss > CR).

Two apparent differences between the study of Godwin et al. (2015) and our study are the somatosensory versus visual modality and the use of a masking paradigm (Godwin et al.) as opposed to near-threshold stimuli. However, assuming that the connectivity changes observed by Godwin et al. are related to the conscious experience, it is difficult to see why those differences should explain the different results. One possible reason why Godwin et al. observed whole-brain network topology alterations for visual awareness might be the unbalanced physical similarity between aware and unaware trials. Hits and misses originated from two different masking conditions: backward masking generated 83% of all hits and forward masking 84% of all misses. Additionally, their total number of trials for 24 participants was not balanced (276 confident misses vs. 486 confident hits). In contrast, our study did not rely on masking the target stimulus and resulted in a balanced total amount of 882 confident misses and 870 confident hits for 31 participants (Figure 8, 10). Furthermore, we also present the results of 1507 hits, and 1190 misses independent of the confidence rating (Figure 10, 11). Future studies investigating visual awareness may be able to distill conscious percepts for present stimuli without confounding masking conditions, for instance taking advantage of sub-millisecond precision of modern tachistoscopes (Sperdin et al., 2013). Awaiting such studies as well as further studies on the somatosensory system and acknowledging – of course – that “absence of proof” is not

826 “proof of absence” – our study cannot provide support for changes in graph metrics with
827 awareness.

828 In summary (integrating our previous findings on the effect of subthreshold
829 stimulation (Blankenburg et al., 2003; Taskin et al., 2008), there seem to be three
830 discernable stages of fMRI-BOLD signal changes with increasing somatosensory stimulus
831 intensity: (i) A deactivation of S1, S2 following (trains of) subthreshold (never-detected)
832 stimuli, (ii) activation of S1, S2, and insula following near-threshold not-detected stimuli,
833 (iii) additional activation of S1, S2 accompanied by activation of a fronto-parietal (likely to
834 be domain-general) network when stimuli are consciously perceived. The potentially
835 differential contribution of the involved brain areas to the conscious experience should be
836 subject to future investigations in which modulations of different aspects of the tasks (e.g.,
837 varying delay, way of report, design e.g., 2AFC versus yes/no task) may be employed. Our
838 study could not confirm changes in graph metrics with awareness for the somatosensory
839 system. Whether this is related to the specific somatosensory modality (electrical nerve
840 stimulation) or the weak stimulation should be investigated by future studies. We think that
841 the data of electrical finger nerve stimulation - despite its limited spatial extent - is a useful
842 model for a range of somatosensory receptors in the fingers, because the nerve
843 integrating the receptor signals is directly stimulated. This view is also supported by similar
844 topographical activation patterns for passive proprioceptive stimulation compared with
845 tactile stimulation (Nasrallah et al., 2019). The potentially differential contribution of the
846 involved brain areas to the conscious experience of electrical stimuli is in line with global
847 broadcasting of individual content of consciousness across the brain without substantial
848 reconfiguration of the brain's network topology resulting in an integrative conscious
849 experience - at least for the observed somatosensory submodality.

References

Aru, J., Bachmann, T., Singer, W., Melloni, L., 2012. Distilling the neural correlates of consciousness. Neuroscience and Biobehavioral Reviews 36, 737–746. doi:10.1016/j.neubiorev.2011.12.003

Auksztulewicz, R., Spitzer, B., Blankenburg, F., 2012. Recurrent neural processing and somatosensory awareness. J Neurosci 32, 799–805. doi:10.1523/JNEUROSCI.3974-11.2012

Baars, B.J., 1988. A cognitive theory of consciousness. Cambridge [England] ; New York : Cambridge University Press.

Bassett, D.S., Sporns, O., 2017. Network neuroscience. Nat Neurosci 20, 353–364. doi:10.1038/nn.4502

Benjamini, Y., Hochberg, Y., 1995. Controlling the False Discovery Rate: A Practical and Powerful Approach to Multiple Testing. Royal Statistical Society, Series B Methodological 57, 289–300. doi:10.2307/2346101

Bisenius, S., Trapp, S., Neumann, J., Schroeter, M.L., 2015. Identifying neural correlates of visual consciousness with ALE meta-analyses. NeuroImage 122, 177–187. doi:10.1016/j.neuroimage.2015.07.070

Blankenburg, F., Ruff, C.C., Deichmann, R., Rees, G., Driver, J., 2006. The cutaneous rabbit illusion affects human primary sensory cortex somatotopically. PLoS Biol 4, e69. doi:10.1371/journal.pbio.0040069

Blankenburg, F., Taskin, B., Ruben, J., Moosmann, M., Ritter, P., Curio, G., Villringer, A., 2003. Imperceptible stimuli and sensory processing impediment. Science 299, 1864–1864. doi:10.1126/science.1080806

Boly, M., Massimini, M., Tsuchiya, N., Postle, B.R., Koch, C., Tononi, G., 2017. Are the Neural Correlates of Consciousness in the Front or in the Back of the Cerebral Cortex? Clinical and Neuroimaging Evidence. J Neurosci 37, 9603–9613. doi:10.1523/JNEUROSCI.3218-16.2017

Bullmore, E.T., Bassett, D.S., 2011. Brain graphs: graphical models of the human brain connectome. Annu Rev Clin Psychol 7, 113–140. doi:10.1146/annurev-clinpsy-040510-143934

874 Casali, A.G., Gosseries, O., Rosanova, M., Boly, M., Sarasso, S., Casali, K.R., Casarotto, S., Bruno, M.-A.,
875 Laureys, S., Tononi, G., Massimini, M., 2013. A Theoretically Based Index of Consciousness
876 Independent of Sensory Processing and Behavior. Science Translational Medicine 5, 198ra105–
877 198ra105. doi:10.1126/scitranslmed.3006294
878 Chen, G., Saad, Z.S., Nath, A.R., Beauchamp, M.S., Cox, R.W., 2012. FMRI group analysis combining effect
879 estimates and their variances. NeuroImage 60, 747–765. doi:10.1016/j.neuroimage.2011.12.060
880 Cisler, J.M., Bush, K., Steele, J.S., 2014. A comparison of statistical methods for detecting context-
881 modulated functional connectivity in fMRI. NeuroImage 84, 1042–1052.
882 doi:10.1016/j.neuroimage.2013.09.018
883 Cole, M.W., Reynolds, J.R., Power, J.D., Repovs, G., Anticevic, A., Braver, T.S., 2013. Multi-task
884 connectivity reveals flexible hubs for adaptive task control. Nat Neurosci 16, 1348–1355.
885 doi:10.1038/nn.3470
886 Cox, R.W., 1996. AFNI: software for analysis and visualization of functional magnetic resonance
887 neuroimages. Comput. Biomed. Res. 29, 162–173. doi:10.1006/cbmr.1996.0014
888 Cox, R.W., Chen, G., Glen, D.R., Reynolds, R.C., Taylor, P.A., 2017. FMRI Clustering in AFNI: False-
889 Positive Rates Redux. Brain Connectivity 7, 152–171. doi:10.1089/brain.2016.0475
890 Dehaene, S., Changeux, J.-P., 2011. Experimental and theoretical approaches to conscious processing.
891 Neuron 70, 200–227. doi:10.1016/j.neuron.2011.03.018
892 Dehaene, S., Changeux, J.-P., Naccache, L., Sackur, J., Sergent, C., 2006. Conscious, preconscious, and
893 subliminal processing: a testable taxonomy. Trends Cogn Sci 10, 204–211.
894 doi:10.1016/j.tics.2006.03.007
895 De Ridder, D., Van Laere, K., Dupont, P., Menovsky, T., Van de Heyning, P., 2007. Visualizing out-of-body
896 experience in the brain. N. Engl. J. Med. 357, 1829–1833. doi:10.1056/NEJMoa070010
897 Eickhoff, S.B., Stephan, K.E., Mohlberg, H., Grefkes, C., Fink, G.R., Amunts, K., Zilles, K., 2005. A new SPM
898 toolbox for combining probabilistic cytoarchitectonic maps and functional imaging data. NeuroImage 25,
899 1325–1335. doi:10.1016/j.neuroimage.2004.12.034
900 Eklund, A., Nichols, T.E., Knutsson, H., 2016. Cluster failure: Why fMRI inferences for spatial extent have
901 inflated false-positive rates. Proc. Natl. Acad. Sci. U.S.A. 113, 7900–7905.
902 doi:10.1073/pnas.1602413113
903 Fischl, B., 2012. FreeSurfer. NeuroImage 62, 774–781. doi:10.1016/j.neuroimage.2012.01.021

904 Forschack, N., Nierhaus, T., Müller, M.M., Villringer, A., 2020. Dissociable neural correlates of stimulation
905 intensity and detection in somatosensation. NeuroImage 116908.
906 doi:10.1016/j.neuroimage.2020.116908
907 Forschack, N., Nierhaus, T., Müller, M.M., Villringer, A., 2017. Alpha-Band Brain Oscillations Shape the
908 Processing of Perceptible as well as Imperceptible Somatosensory Stimuli during Selective Attention. J
909 Neurosci 37, 6983–6994. doi:10.1523/JNEUROSCI.2582-16.2017
910 Frässle, S., Sommer, J., Jansen, A., Naber, M., Einhäuser, W., 2014. Binocular rivalry: frontal activity relates
911 to introspection and action but not to perception. J Neurosci 34, 1738–1747.
912 doi:10.1523/JNEUROSCI.4403-13.2014
913 Friston, K.J., Williams, S., Howard, R., Frackowiak, R.S., Turner, R., 1996. Movement-related effects in fMRI
914 time-series. Magn. Reson. Med. 35, 346–355.
915 Frith, C.D., 2019. The neural basis of consciousness. Psychol Med 133, 1–13.
916 doi:10.1017/S0033291719002204
917 Garrison, K.A., Scheinost, D., Finn, E.S., Shen, X., Constable, R.T., 2015. The (in)stability of functional brain
918 network measures across thresholds. NeuroImage 118, 651–661.
919 doi:10.1016/j.neuroimage.2015.05.046
920 Gitelman, D.R., Penny, W.D., Ashburner, J., Friston, K.J., 2003. Modeling regional and psychophysiologic
921 interactions in fMRI: the importance of hemodynamic deconvolution. NeuroImage 19, 200–207.
922 doi:10.1016/S1053-8119(03)00058-2
923 Glasser, M.F., Coalson, T.S., Robinson, E.C., Hacker, C.D., Harwell, J., Yacoub, E., Ugurbil, K., Andersson,
924 J., Beckmann, C.F., Jenkinson, M., Smith, S.M., Van Essen, D.C., 2016. A multi-modal parcellation of
925 human cerebral cortex. Nature 536, 171–178. doi:10.1038/nature18933
926 Godwin, D., Barry, R.L., Marois, R., 2015. Breakdown of the brain's functional network modularity with
927 awareness. Proc. Natl. Acad. Sci. U.S.A. 112, 3799–3804. doi:10.1073/pnas.1414466112
928 Guimerà, R., Nunes Amaral, L.A., 2005. Functional cartography of complex metabolic networks. Nature 433,
929 895–900. doi:10.1038/nature03288
930 Hirvonen, J., Palva, S., 2016. Cortical localization of phase and amplitude dynamics predicting access to
931 somatosensory awareness. Hum Brain Mapp 37, 311–326. doi:10.1002/hbm.23033
932 Ionta, S., Martuzzi, R., Salomon, R., Blanke, O., 2014. The brain network reflecting bodily self-
933 consciousness: a functional connectivity study. Soc Cogn Affect Neurosci 9, 1904–1913.
934 doi:10.1093/scan/nst185
935 Kingdom, F.A.A., Prins, N., 2009. Psychophysics. Academic Press Inc, London.

936 Kleiner, M., Brainard, D., Pelli, D., Ingling, A., Murray, R., Broussard, C., 2007. What's new in psychtoolbox-
937 3. Perception 36, 1–16.
938 Koch, C., Massimini, M., Boly, M., Tononi, G., 2016. Neural correlates of consciousness: progress and
939 problems. Nat Rev Neurosci 17, 307–321. doi:10.1038/nrn.2016.22
940 Lamme, V.A.F., 2006. Towards a true neural stance on consciousness. Trends Cogn Sci 10, 494–501.
941 doi:10.1016/j.tics.2006.09.001
942 Martuzzi, R., van der Zwaag, W., Dieguez, S., Serino, A., Gruetter, R., Blanke, O., 2015. Distinct
943 contributions of Brodmann areas 1 and 2 to body ownership. Soc Cogn Affect Neurosci 10, 1449–1459.
944 doi:10.1093/scan/nsv031
945 Mashour, G.A., Roelfsema, P., Changeux, J.-P., Dehaene, S., 2020. Conscious Processing and the Global
946 Neuronal Workspace Hypothesis. Neuron 105, 776–798. doi:10.1016/j.neuron.2020.01.026
947 McLaren, D.G., Ries, M.L., Xu, G., Johnson, S.C., 2012. A generalized form of context-dependent
948 psychophysiological interactions (gPPI): a comparison to standard approaches. NeuroImage 61, 1277–
949 1286. doi:10.1016/j.neuroimage.2012.03.068
950 Moeller, S., Yacoub, E., Olman, C.A., Auerbach, E., Strupp, J., Harel, N., Ugurbil, K., 2010. Multiband
951 multislice GE-EPI at 7 tesla, with 16-fold acceleration using partial parallel imaging with application to
952 high spatial and temporal whole-brain fMRI. Magn. Reson. Med. 63, 1144–1153.
953 doi:10.1002/mrm.22361
954 Moore, C.I., Crosier, E., Greve, D.N., Savoy, R., Merzenich, M.M., Dale, A.M., 2013. Neocortical correlates
955 of vibrotactile detection in humans. J Cognitive Neurosci 25, 49–61. doi:10.1162/jocn_a_00315
956 Morey, R.D., 2008. Confidence Intervals from Normalized Data: A correction to Cousineau (2005). Tutor
957 Quant Methods Psychol 61–64.
958 Naghavi, H.R., Nyberg, L., 2005. Common fronto-parietal activity in attention, memory, and consciousness:
959 Shared demands on integration? Conscious Cogn 14, 390–425. doi:10.1016/j.concog.2004.10.003
960 Nasrallah, F.A., Mohamed, A.Z., Campbell, M.E., Yap, H.K., Yeow, C.-H., Lim, J.H., 2019. Functional
961 connectivity of brain associated with passive range of motion exercise: Proprioceptive input promoting
962 motor activation? NeuroImage 202, 116023. doi:10.1016/j.neuroimage.2019.116023
963 Newman, M.E.J., 2004. Analysis of weighted networks. Phys. Rev. E 70, 056131.
964 doi:10.1103/PhysRevE.70.056131
965 Nierhaus, T., Forschack, N., Piper, S.K., Holtze, S., Krause, T., Taskin, B., Long, X., Stelzer, J., Margulies,
966 D.S., Steinbrink, J., Villringer, A., 2015. Imperceptible somatosensory stimulation alters sensorimotor

967 background rhythm and connectivity. J Neurosci 35, 5917–5925. doi:10.1523/JNEUROSCI.3806-
968 14.2015
969 Oldfield, R.C., 1971. The assessment and analysis of handedness: the Edinburgh inventory.
970 Neuropsychologia 9, 97–113. doi:10.1016/0028-3932(71)90067-4
971 Onnela, J.-P., Saramäki, J., Kertész, J., Kaski, K., 2005. Intensity and coherence of motifs in weighted
972 complex networks. Phys. Rev. E 71, 065103. doi:10.1103/PhysRevE.71.065103
973 O'Reilly, J.X., Woolrich, M.W., Behrens, T.E.J., Smith, S.M., Johansen-Berg, H., 2012. Tools of the trade:
974 psychophysiological interactions and functional connectivity. Soc Cogn Affect Neurosci 7, 604–609.
975 doi:10.1093/scan/nss055
976 Park, H.-D., Blanke, O., 2019. Coupling Inner and Outer Body for Self-Consciousness. Trends Cogn Sci 23,
977 377–388. doi:10.1016/j.tics.2019.02.002
978 Power, J.D., Barnes, K.A., Snyder, A.Z., Schlaggar, B.L., Petersen, S.E., 2012. Spurious but systematic
979 correlations in functional connectivity MRI networks arise from subject motion. NeuroImage 59, 2142–
980 2154. doi:10.1016/j.neuroimage.2011.10.018
981 Power, J.D., Cohen, A.L., Nelson, S.M., Wig, G.S., Barnes, K.A., Church, J.A., Vogel, A.C., Laumann, T.O.,
982 Miezin, F.M., Schlaggar, B.L., Petersen, S.E., 2011. Functional network organization of the human
983 brain. Neuron 72, 665–678. doi:10.1016/j.neuron.2011.09.006
984 Preusser, S., Thiel, S.D., Rook, C., Roggenhofer, E., Kosatschek, A., Draganski, B., Blankenburg, F., Driver,
985 J., Villringer, A., Pleger, B., 2015. The perception of touch and the ventral somatosensory pathway.
986 Brain 138, 540–548. doi:10.1093/brain/awu370
987 Rajaei, N., Aoki, N., Takahashi, H.K., Miyaoka, T., Kochiyama, T., Ohka, M., Sadato, N., Kitada, R., 2018.
988 Brain networks underlying conscious tactile perception of textures as revealed using the velvet hand
989 illusion. Hum Brain Mapp 39, 4787–4801. doi:10.1002/hbm.24323
990 Rees, G., Kreiman, G., Koch, C., 2002. Neural correlates of consciousness in humans. Nat Rev Neurosci 3,
991 261–270. doi:10.1038/nrn783
992 Roland, P.E., 1987. Somatosensory detection in patients with circumscribed lesions of the brain. Exp Brain
993 Res 66, 303–317. doi:10.1007/BF00243307
994 Ronchi, R., Bello-Ruiz, J., Lukowska, M., Herbelin, B., Cabrilo, I., Schaller, K., Blanke, O., 2015. Right
995 insular damage decreases heartbeat awareness and alters cardio-visual effects on bodily self-
996 consciousness. Neuropsychologia 70, 11–20. doi:10.1016/j.neuropsychologia.2015.02.010
997 Rorden, C., Brett, M., 2000. Stereotaxic display of brain lesions. Behav Neurol 12, 191–200.

998 Rouder, J.N., Morey, R.D., Speckman, P.L., Province, J.M., 2012. Default Bayes factors for ANOVA designs.
999 Journal of Mathematical Psychology 56, 356–374. doi:10.1016/j.jmp.2012.08.001
1000 Ruben, J., Schwiemann, J., Deuchert, M., Meyer, R., Krause, T., Curio, G., Villringer, K., Kurth, R., Villringer,
1001 A., 2001. Somatotopic organization of human secondary somatosensory cortex. Cereb Cortex 11, 463–
1002 473.
1003 Rubinov, M., Sporns, O., 2010. Complex network measures of brain connectivity: uses and interpretations.
1004 NeuroImage 52, 1059–1069. doi:10.1016/j.neuroimage.2009.10.003
1005 Sadaghiani, S., Poline, J.-B., Kleinschmidt, A., D'Esposito, M., 2015. Ongoing dynamics in large-scale
1006 functional connectivity predict perception. Proc. Natl. Acad. Sci. U.S.A. 112, 8463–8468.
1007 doi:10.1073/pnas.1420687112
1008 Schmidt, T.T., Blankenburg, F., 2018. Brain regions that retain the spatial layout of tactile stimuli during
1009 working memory - A 'tactospatial sketchpad'? NeuroImage 178, 531–539.
1010 doi:10.1016/j.neuroimage.2018.05.076
1011 Schönbrodt, F.D., Wagenmakers, E.-J., 2018. Bayes factor design analysis: Planning for compelling
1012 evidence. Psychon Bull Rev 25, 128–142. doi:10.3758/s13423-017-1230-y
1013 Schröder, P., Schmidt, T.T., Blankenburg, F., 2019. Neural basis of somatosensory target detection
1014 independent of uncertainty, relevance, and reports. eLife 8, 34. doi:10.7554/eLife.43410
1015 Schubert, R., Blankenburg, F., Lemm, S., Villringer, A., Curio, G., 2006. Now you feel it-now you don't: ERP
1016 correlates of somatosensory awareness. Psychophysiology 43, 31–40. doi:10.1111/j.1469-
1017 8986.2006.00379.x

1018 Setsompop, K., Gagoski, B.A., Polimeni, J.R., Witzel, T., Wedeen, V.J., Wald, L.L., 2012. Blipped-controlled
1019 aliasing in parallel imaging for simultaneous multislice echo planar imaging with reduced g-factor
1020 penalty. Magn. Reson. Med. 67, 1210–1224. doi:10.1002/mrm.23097
1021 Smith, S.M., Jenkinson, M., Woolrich, M.W., Beckmann, C.F., Behrens, T.E.J., Johansen-Berg, H.,
1022 Bannister, P.R., De Luca, M., Drobnjak, I., Flitney, D.E., Niazy, R.K., Saunders, J., Vickers, J., Zhang,
1023 Y., De Stefano, N., Brady, J.M., Matthews, P.M., 2004. Advances in functional and structural MR image
1024 analysis and implementation as FSL. NeuroImage 23 Suppl 1, S208–19.
1025 doi:10.1016/j.neuroimage.2004.07.051
1026 Sperdin, H.F., Repnow, M., Herzog, M.H., Landis, T., 2013. An LCD tachistoscope with submillisecond
1027 precision. Behav Res Methods 45, 1347–1357. doi:10.3758/s13428-012-0311-0
1028 Taskin, B., Holtze, S., Krause, T., Villringer, A., 2008. Inhibitory impact of subliminal electrical finger
1029 stimulation on SI representation and perceptual sensitivity of an adjacent finger. NeuroImage 39, 1307–
1030 1313. doi:10.1016/j.neuroimage.2007.09.039
1031 van Gaal, S., Lamme, V.A.F., 2012. Unconscious high-level information processing: implication for
1032 neurobiological theories of consciousness. Neuroscientist 18, 287–301.
1033 doi:10.1177/1073858411404079
1034 Vatansever, D., Menon, D.K., Manktelow, A.E., Sahakian, B.J., Stamatakis, E.A., 2015. Default Mode
1035 Dynamics for Global Functional Integration. J Neurosci 35, 15254–15262.
1036 doi:10.1523/JNEUROSCI.2135-15.2015
1037 Weisz, N., Wühle, A., Monittola, G., Demarchi, G., Frey, J., Popov, T., Braun, C., 2014. Prestimulus
1038 oscillatory power and connectivity patterns predispose conscious somatosensory perception. Proc. Natl.
1039 Acad. Sci. U.S.A. 111, E417–25. doi:10.1073/pnas.1317267111
1040 Xia, M., Wang, J., He, Y., 2013. BrainNet Viewer: a network visualization tool for human brain connectomics.
1041 PLoS ONE 8, e68910. doi:10.1371/journal.pone.0068910